



POLITECNICO
MILANO 1863

**SCUOLA DI INGEGNERIA INDUSTRIALE
E DELL'INFORMAZIONE**

EXECUTIVE SUMMARY OF THE THESIS

A multi-physics oxygenation model: from biological derivation to the numerical simulation of real-life scenarios

LAUREA MAGISTRALE IN MATHEMATICAL ENGINEERING - INGEGNERIA MATEMATICA

Author: MANFRED NESTI

Advisor: DR. FRANCESCO REGAZZONI

Co-advisors: DR. PASQUALE CLAUDIO AFRICA, DR. IVAN FUMAGALLI

Academic year: 2021-2022

1. Introduction

The myocardium requires a continuous oxygen supply to work properly: oxygenated blood reaches the heart through the coronaries and perfuses the whole muscular tissue, allowing the exchange of oxygen at the microvasculature level. Oxygen delivery can be jeopardized due to reduced flow either because of coronary arteries obstructions, aortic valve regurgitation, or left ventricular hypertrophy, as well as in the case of pathologies such as SARS-CoV-2 infection [7]. The iHEART project represents one of the first attempts in the world to create a complete mathematical model of the human heart and aims to build a digital-twin capable of describing in detail the interactions that take place within it.

This thesis aims at extending the project computational toolbox by introducing an innovative mathematical model of cardiac oxygenation capable of simulating the space-time evolution of quantities such as saturation and oxygen concentration within the cardiac capillaries and muscle tissue. In this work, the oxygenation model is coupled with models governing the fluid dynamics of blood in the coronary arteries and gradually smaller vessels through a perfusion model. The equations characterizing the oxygenation model and their coupling with the other physics were discretized and implemented within the life^x cardiac simulation library [1].

After a careful calibration of the physical parameters so that the model fully reflects the real scenar-

ios, we tested the model through simulations on idealized coronary and myocardial geometries. Finally, through simulations on real geometries, we simulated physiological and pathological scenarios (i.e., patient with SARS-CoV-2 infection), both in the case of a patient at rest and under stress, confirming that the model is in agreement with the literature and an interesting improvement of the state of the art.

In the last decades, several authors have developed different mathematical and numerical models to understand these phenomena better.

Di Gregorio et al. [3] provide a helpful literature review of models for blood dynamics in epicardial coronary arteries, such as Poiseuille's law, lumped parameter models and Navier-Stokes equations, and in intramural coronary vessels, as the multi-compartment Darcy model in which the myocardium is divided into co-existing compartments corresponding to different length scales.

Goldman [4] provides a literature review of mathematical models for oxygen exchange, such as the Krogh model and its variants, to study blood-tissue oxygen transport and release into the tissue.

2. Mathematical models

2.1. Blood dynamics in epicardial coronary arteries

The blood dynamics in the epicardial coronary artery domain Ω_C is modeled through the Navier-Stokes equations for an incompressible, homogeneous, and Newtonian fluid under the assumption of rigid walls. The equations are

$$\rho \left(\frac{\partial \mathbf{u}_C}{\partial t} + (\mathbf{u}_C \cdot \nabla) \mathbf{u}_C \right) - \mu_C \nabla \cdot (\nabla \mathbf{u}_C + (\nabla \mathbf{u}_C)^T) + \nabla p_C = \mathbf{0} \text{ in } \Omega_C, \quad (1a)$$

$$\nabla \cdot \mathbf{u}_C = 0 \text{ in } \Omega_C, \quad (1b)$$

$$\mathbf{u}_C = \mathbf{0} \text{ on } \Gamma_w, \quad (1c)$$

$$\mathbf{u}_C = \mathbf{u}_{in} \text{ on } \Gamma_{in}, \quad (1d)$$

where \mathbf{u}_C (m s^{-1}) and p_C (mmHg) are the blood velocity and pressure, respectively, in the epicardial coronary arteries, ρ (kg m^{-3}) the blood density, μ_C (mmHg s) the blood viscosity; Γ_w is the lateral physical vessel wall with a no-slip condition, and Γ_{in} is the inlet section representing the coronary left and right ostia located at the aortic root, where a physiological velocity profile \mathbf{u}_{in} is imposed. Some reasonable physiological values for the involved parameters, such as the input velocity profile \mathbf{u}_{in} , are provided in [3].

2.2. Blood dynamics in intramural coronary vessels

For our purposes, we represent intramural vessels employing three compartments co-existing in the myocardium Ω_M , in which the vessels have a diameter in the range of $\sim 200 \text{ }\mu\text{m} \div 1 \text{ mm}$ for large vessel ($i = 1$); $\sim 60 \div 200 \text{ mm}$ for mid-size vessels ($i = 2$) and $\sim 5 \div 60 \text{ }\mu\text{m}$ for the microvasculature ($i = 3$). The strong primal formulation of three-compartments Darcy model, in which we eliminated velocity, is written in terms of only pressure variables p_i and it reads

$$\begin{aligned} -\nabla \cdot (\mathbf{K}_1 \cdot \nabla p_1) &= g_1 - \beta_{1,2}(p_1 - p_2) && \text{in } \Omega_M, & (2a) \\ \mathbf{u}_1 \cdot \mathbf{n} &= 0 && \text{on } \partial\Omega_M, & (2b) \\ -\nabla \cdot (\mathbf{K}_2 \cdot \nabla p_2) &= -\beta_{2,1}(p_2 - p_1) - \beta_{2,3}(p_2 - p_3) && \text{in } \Omega_M, & (2c) \\ \mathbf{u}_2 \cdot \mathbf{n} &= 0 && \text{on } \partial\Omega_M, & (2d) \\ -\nabla \cdot (\mathbf{K}_3 \cdot \nabla p_3) &= -\gamma(p_3 - p_{veins}) - \beta_{3,2}(p_3 - p_2) && \text{in } \Omega_M, & (2e) \\ \mathbf{u}_3 \cdot \mathbf{n} &= 0 && \text{on } \partial\Omega_M, & (2f) \end{aligned}$$

where in compartment i , \mathbf{u}_i denotes the blood velocity, p_i is the pore pressure, \mathbf{K}_i ($\text{m}^2 \text{s}^{-1} \text{ mmHg}^{-1}$) the permeability tensor, g_i (s^{-1}) a volumetric source or sink term and $\beta_{i,k}$ ($\text{s}^{-1} \text{ mmHg}^{-1}$) for $i, k = 1 \dots 3$, represent the inter-compartment pressure coupling coefficients. The first compartment has a source term g_1 depending on the blood dynamics in epicardial coronary arteries and the small-scale compartment has a sink term $-\gamma(p_3 - p_{veins})$ that accounts for coronary venous return, where p_{veins} (Pa) is venous pressure and γ ($\text{s}^{-1} \text{ mmHg}^{-1}$) is a drain coefficient. Some reasonable physiological values for the involved parameters are provided in [3].

2.3. Oxygen exchange in microvasculature

In this section, we physically derived the oxygenation model presented by Regazzoni in [8]. Both with the three compartments denoted by $i = 1, 2, 3$, we consider existing an initial compartment $i = a$ representing the arterial blood, and a final one $i = m$ downstream from these, representing the cardiac muscle. We denote by ψ_i (–) and by $\phi_{i,j}$ (s^{-1}) the volume fraction occupied by compartment i and the volume flux per unit volume of tissue between compartments i, j respectively. We assume that in the compartment $i = a$, the chemical reactions are in equilibrium and that PO_2^a is a given datum (constant in time), it is possible to prove that, in the compartments $i = 1, 2$, saturation and partial oxygen pressure do not change with respect to arterial blood: therefore, we focus on compartment $i = 3$. From now on, we will use the notation $[X]$ (mol m^{-3}) to denote the concentration of specie X in the blood. The model concerns the dynamics of oxygen concentration in capillaries $[\text{O}_2^*]$ and partial pressure of oxygen in the myocardium PO_2^m (mmHg). Other involved quantities are the oxygen saturation in capillaries SO_2 (–) given by

$$\text{SO}_2^i = \left(1 + \left(\frac{\text{PO}_2^{50}}{\text{PO}_2^i} \right)^n \right)^{-1}, \quad (3a)$$

and oxygen partial pressure in capillaries PO_2 (mmHg) we can obtain from

$$[\text{O}_2^*]^3 = n[\text{Hb}^*] \left(1 + \left(\frac{\text{PO}_2^{50}}{\text{PO}_2^3} \right)^n \right)^{-1} + \alpha^{-1} \text{PO}_2^3 =: g(\text{PO}_2^3), \quad (4a)$$

where n (–) is the hemoglobin's number sites for oxygen, α ($\text{mmHg m}^3 \text{ mol}^{-1}$) is the Henry law's constant, $[\text{Hb}^*]$ is the concentration of total hemoglobin, and $\text{PO}_2^{m,50}$ (mmHg) is the half maximal effective partial pressure of oxygen.

We assume that the oxygen-hemoglobin association/dissociation chemical reaction is much faster than the other phenomena, which are in turn to be considered at equilibrium: we will refer to this model as the reduced model, with respect to the complete one, where no such assumption is made. The model's equations depend on chemical reactions, advection, diffusion, and flux from and to neighboring compartments. We assume that the vascular membrane is permeable to oxygen but not hemoglobin, that oxygen is exchanged only by the third compartment, and that blood always flows downstream. The dynamics of PO_2^m are modeled using the Michaelis-Menten dynamics depending on the parameter ξ_0 ($\text{mol m}^{-3} \text{ s}^{-1}$), which is the maximum oxygen consumption rate. The reduced model is

$$\begin{aligned} \frac{\partial}{\partial t} [\text{O}_2^*]^3 + \psi_3^{-1} \nabla \cdot ([\text{O}_2^*]^3 \mathbf{u}_3) + \mu \Delta [\text{O}_2^*]^3 &= \psi_3^{-1} \hat{\phi}_{3,3} [\text{O}_2^*]^2 \\ &\quad - \psi_3^{-1} \hat{\phi}_{3,veins} [\text{O}_2^*]^3 \\ &\quad - \psi_3^{-1} \bar{P} \alpha^{-1} (g^{-1}([\text{O}_2^*]^3) - \text{PO}_2^m), \end{aligned} \quad (5a)$$

$$\begin{aligned} \frac{\partial}{\partial t} \text{PO}_2^m &= \psi_m^{-1} \bar{P} (g^{-1}([\text{O}_2^*]^3) - \text{PO}_2^m) \\ &\quad - \tilde{\xi}_0 \left(1 + \left(\frac{\text{PO}_2^{50}}{\text{PO}_2^m} \right)^n \right)^{-1}, \end{aligned} \quad (5b)$$

where k_+, k_- (s^{-1}) are the association/dissociation rate constant, and \tilde{P} ($\text{m}^3 \text{s}^{-1} \text{m}^{-2}$) is the effective permeability. The values of the parameters characterizing the equations in physiological scenario are provided in [6] or calibrated by experimental measures, except for μ , which is arbitrarily set to $0.1 \text{ m}^2 \text{s}^{-1}$. We also define the average amount of oxygen delivered from capillaries to the muscle and consumed to the muscle to produce ATP as $\lambda_{\text{O}_2}^{\text{del}}(t)$ and $\lambda_{\text{O}_2}^{\text{cons}}(t)$ (mol m^{-3}), both with their time integrals: the total amount of these quantities $\Lambda_{\text{O}_2}^{\text{del}}(t)$ and $\Lambda_{\text{O}_2}^{\text{cons}}(t)$ ($\text{mol m}^{-3} \text{s}^{-1}$).

$$\lambda_{\text{O}_2}^{\text{del}}(t) = \frac{1}{|\Omega_M|} \int_{\Omega_M} \tilde{P} \alpha^{-1} (g^{-1} ([\text{O}_2^*]^3) - \text{PO}_2^m) d\omega, \quad (6a)$$

$$\lambda_{\text{O}_2}^{\text{cons}}(t) = \frac{1}{|\Omega_M|} \int_{\Omega_M} \psi_m \tilde{\xi}_0 \alpha^{-1} \left(1 + \frac{\text{PO}_2^{m,50}}{\text{PO}_2^m} \right)^{-1} d\omega \quad (6b)$$

$$\Lambda_{\text{O}_2}^{\text{del}}(t) = \int_0^t \lambda_{\text{O}_2}^{\text{del}}(u) du, \quad \Lambda_{\text{O}_2}^{\text{cons}}(t) = \int_0^t \lambda_{\text{O}_2}^{\text{cons}}(u) du. \quad (6c)$$

The averaged flux of blood flowing from the compartment $i-1$ to i inside a tissue myocardium volume Ω_M , and during a heart cycle $[0, T]$ is the average CBF, and can its typical value is known to be nearly $0.8 \text{ mL min}^{-1} \text{ g}^{-1}$ [6].

2.4. Coupling conditions

The coupling between the three models is summarized in Figure 1: we simulate the blood fluid dynamics in the coronaries coupled with the blood perfusion in the myocardium as a porous medium, and finally, we use the perfusion output as input of the oxygenation model to compute the desired quantities.

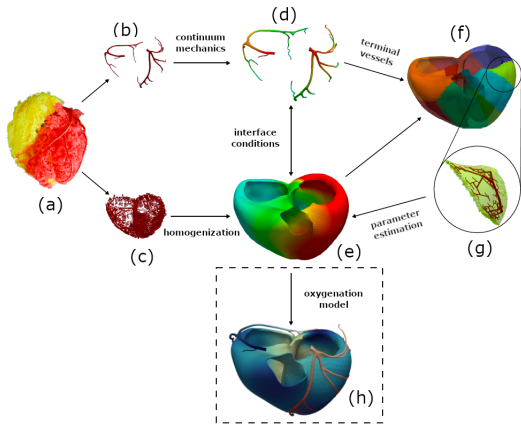


Figure 1: Design of multi-physics oxygenation model.

To couple the fluid dynamics and perfusion models, we assume that there is a one-to-one correspondence between outlets of epicardial coronary arteries and perfusion regions $\Omega_M^j, j = 1, \dots, J$, where the exchange of information between epicardial coronary arteries and intramural vessels occurs. The coupling occurs at multiple levels: directly, through interface conditions based on the continuity of mass and momentum, and indirectly, through the virtual network

of intramural vessels. We assume that tangential tractions are null.

The vector field \mathbf{u}_3 and the scalar fields $\hat{\phi}_{2,3}$ and $\hat{\phi}_{3,\text{veins}}$ are responsible for the coupling with fluid and perfusion problems. In case we want to use the oxygenation model uncoupled from the others, we adopted $\mathbf{u}_3 = \mathbf{0}$ and spatially homogeneous blood fluxes sinusoidally in time that provide $\bar{\Psi}_{\text{CBF}} = 0.63 \text{ mL min}^{-1} \text{ g}^{-1}$ in accordance with the literature. To couple the oxygenation model with the three-compartment Darcy model, we set

$$\mathbf{u}_3 = -\mathbf{K}_3 \nabla p_3, \quad \hat{\phi}_{2,3} = \beta_{2,3}(p_3 - p_2), \quad \hat{\phi}_{3,\text{veins}} = \gamma(p_3 - p_{\text{veins}}). \quad (7a)$$

With the coupling conditions above, the three-compartment multi-physics problem (1)–(2)–(5) is the following.

$$\rho \left(\frac{\partial \mathbf{u}_C}{\partial t} + (\mathbf{u}_C \cdot \nabla) \mathbf{u}_C \right) \quad (8a)$$

$$-\mu_C \nabla \cdot (\nabla \mathbf{u}_C + (\nabla \mathbf{u}_C)^T) + \nabla p_C = \mathbf{0} \text{ in } \Omega_C, \quad (8b)$$

$$\nabla \cdot \mathbf{u}_C = \mathbf{0} \text{ in } \Omega_C, \quad (8c)$$

$$p_C - \mu_C (\nabla \mathbf{u}_C + (\nabla \mathbf{u}_C)^T) \mathbf{n} \cdot \mathbf{n} = -\frac{1}{\alpha^j} \int_{\Gamma^j} \mathbf{u}_C \cdot \mathbf{n} d\gamma = \frac{1}{|\Omega_M^j|} \int_{\Omega_M^j} p_1 d\omega \text{ on } \Gamma^j, \quad (8d)$$

$$\mu_C (\nabla \mathbf{u}_C + (\nabla \mathbf{u}_C)^T) \mathbf{n} \cdot \tau_i = 0, \quad i = 1, 2 \text{ on } \Gamma^j, \quad (8e)$$

$$\mathbf{u}_1 + \mathbf{K}_1 \nabla p_1 = \mathbf{0} \text{ in } \Omega_M, \quad (8f)$$

$$\nabla \cdot \mathbf{u}_1 = \sum_{j=1}^J \frac{\chi_{\Omega_M^j}}{|\Omega_M^j|} \int_{\Gamma^j} \mathbf{u}_C \cdot \mathbf{n} d\gamma - \beta_{1,2}(p_1 - p_2) \text{ in } \Omega_M, \quad (8g)$$

$$\mathbf{u}_2 + \mathbf{K}_2 \nabla p_2 = \mathbf{0} \text{ in } \Omega_M, \quad (8h)$$

$$\nabla \cdot \mathbf{u}_2 = -\beta_{2,1}(p_2 - p_1) - \beta_{2,3}(p_2 - p_3) \text{ in } \Omega_M, \quad (8i)$$

$$\mathbf{u}_3 + \mathbf{K}_3 \nabla p_3 = \mathbf{0} \text{ in } \Omega_M, \quad (8j)$$

$$\nabla \cdot \mathbf{u}_3 = -\gamma(p_3 - p_{\text{veins}}) - \beta_{3,2}(p_3 - p_2) \text{ in } \Omega_M, \quad (8k)$$

$$\mathbf{u}_i \cdot \mathbf{n} = 0, \quad i = 1, 2, 3 \text{ on } \partial \Omega_M, \quad (8l)$$

$$\frac{\partial}{\partial t} [\text{O}_2^*]^3 + \psi_3^{-1} \nabla \cdot (-\mathbf{K}_3 [\text{O}_2^*]^3 \nabla p_3) + \mu \Delta [\text{O}_2^*]^3 = \psi_3^{-1} \beta_{2,3}(p_3 - p_2) [\text{O}_2^*]^2 \quad (8m)$$

$$- \psi_3^{-1} \gamma(p_M, 3 - p_{\text{veins}}) [\text{O}_2^*]^3 \quad (8m)$$

$$- \psi_3^{-1} \tilde{P} \alpha^{-1} (g^{-1} ([\text{O}_2^*]^3) - \text{PO}_2^m) \text{ in } \Omega_M,$$

$$\frac{\partial}{\partial t} \text{PO}_2^m = \psi_m^{-1} \tilde{P} (g^{-1} ([\text{O}_2^*]^3) - \text{PO}_2^m) \quad (8m)$$

$$- \tilde{\xi}_0 \left(1 + \frac{\text{PO}_2^{m,50}}{\text{PO}_2^m} \right)^{-1} \text{ in } \Omega_M. \quad (8m)$$

The problem is completed by computing the other quantities of interest as (6).

3. Numerical schemes

The implementation of the multi-physics model was made inside the life^x, a C++ high-performance finite element library focused on mathematical models and numerical methods for cardiac applications [1]. We leveraged the fluid dynamics and perfusion models already provided, implementing the oxygenation one and the coupling with the former.

For the subproblems regarding fluid dynamics and perfusion, we use the finite-element method with SUPG-SUPG stabilization for spatial discretization and a backward differentiation formula of order 1 for time discretization. Regarding the oxygenation model, we use the space $L_2([0, T], H^1(\Omega_M))$ for $[\text{O}_2^*]$ and PO_2^m . For the space discretization we use a standard Galerkin approximation of the problem,

while regarding the time discretization, we subdivide the time interval $[0, T]$ into $N_{\Delta t}$ subintervals of size $\Delta t = \frac{T}{N_{\Delta t}}$, so that the time steps are defined as $t_k = k\Delta t$ for $k = 0, \dots, N_{\Delta t}$. We use a semi-implicit method for the time discretization scheme, with an implicit treatment for the linear terms and an explicit treatment for the nonlinear terms (i.e., g function) and to decouple the two problems. The algebraic formulation of the discrete problem to be solved for each $k = 0, \dots, N_{\Delta t} - 1$ is

$$\begin{bmatrix} A^k & O \\ O & I \end{bmatrix} \begin{bmatrix} [\text{O}_2^*]^{3,k+1} \\ \text{PO}_2^m,k+1 \end{bmatrix} = \begin{bmatrix} F^k \\ G^k \end{bmatrix}, \quad (9a)$$

where I is the identity matrix and where the submatrix A^k and the subvectors F^k, G^k depends on the timestep k and need to be re-assembled for each timestep. Notice that the algebraic linear system is diagonal since we used an explicit treatment to decouple the two subproblems.

In case we are interested in solving the 0D model, i.e., neglecting the diffusive and transport terms, we proposed a Runge-Kutta explicit scheme of the fourth order. Regarding the average and total fluxes of delivered and consumed oxygen, we leveraged on a trapezoidal integration rule.

Regarding the coupling schemes, for the two-way coupling between the fluid dynamics and the perfusion model, we adopted the same iterative splitting strategy as in [3]. In contrast, for the oxygenation model, we leveraged the fact that it depends only one way from the perfusion one, allowing us to simply compute the quantities of oxygenation model using as input the perfusion model output, as in Algorithm 1.

Algorithm 1 One-way coupling between three-compartment Darcy and oxygenation model

-
- 1: **for** $k = 0, \dots, N_{\Delta t} - 1$ **do**
 - 2: Perform the iterative splitting strategy to solve the fluid and Darcy coupled problems at timestep k .
 - 3: Update the scalar fields (7) at timestep k .
 - 4: Assemble submatrices and subvectors of the oxygenation problem (9) at timestep k .
 - 5: Solve the corresponding algebraic linear system (9).
 - 6: Compute the quantities of interest (3)–(4)–(6).
 - 7: **end for**
-

4. Tests and results

To assess the model validity and its implementation in life^x, we compare different simulations on ideal geometries of coronaries (cylinder) and myocardium (cube). The comparison between the complete and reduced model confirms the validity of the quasistatic-chemistry assumption. Moreover, the complete model requires a smaller timestep to capture the quick chemical reaction adequately. Hence, we only consider the reduced model from now on. The comparison between the 3D and 0D models shows that the 0D model is a good approximation of the 3D one. Finally, the run of the complete model, both in case of simulation of only perfusion or including also the coronaries, confirms the validity of the coupled model and the coupling conditions imposed by numerical schemes.

We also investigated realistic geometries of coronaries and myocardium in some real-life scenarios. In particular, we investigated the oxygenation in a patient under both physiological and pathological (i.e., SARS-CoV-2 infection) conditions and the effects of physical activity on both these cases. The simulations were executed on 56 cores running Intel Xeon Gold 6238@2.10 GHz, using the computational resources available at MOX, Dipartimento di Matematica, Politecnico di Milano.

For this purpose, the geometries of the computational domains Ω_C and Ω_M , describing the epicardial coronary arteries and the myocardium of the left and right ventricles, are defined starting from the 3D Human Heart Model provided by Zygote. The corresponding computational meshes are composed of 726,982 tetrahedral elements for Ω_C and 214,484 hexahedral elements for Ω_M . The domain Ω_M is partitioned into 17 perfusion regions on which the calibrated parameters K_i and $\beta_{i,j}$ take value. At the inlet sections $\Gamma_{in,k}$, $k = l, r$ of the epicardial left ($k = l$) and right ($k = r$) vessel, we prescribe the flow rate condition $\int_{\Gamma_{in,k}} \mathbf{u}_C \cdot \mathbf{n} d\gamma = \Psi_{CBFk}$ for $k = l, r$ and with $\Psi_{CBFl} = 0.57\Psi_{CBF}$, $\Psi_{CBFr} = 0.43\Psi_{CBF}$ and Ψ_{CBF} being the inlet CBF with a physiological profile shown in Figure 2 in scenario of healthy subject. In Figure 2, the blue, red, and green points (reported only in the first period) denote some notable time instants in the simulation: the beginning of the systole, the beginning of the diastole, and the plateau at the end of the diastole, respectively. With this prescription, the average CBF is $\bar{\Psi}_{CBF} = 0.695 \text{ mL min}^{-1} \text{ g}^{-1}$, which is reasonably near to the literature value of 0.8 [2]. In all the simulations, the initial values of PO_2^3 and PO_2^m are tuned to quickly reach a limit cycle.

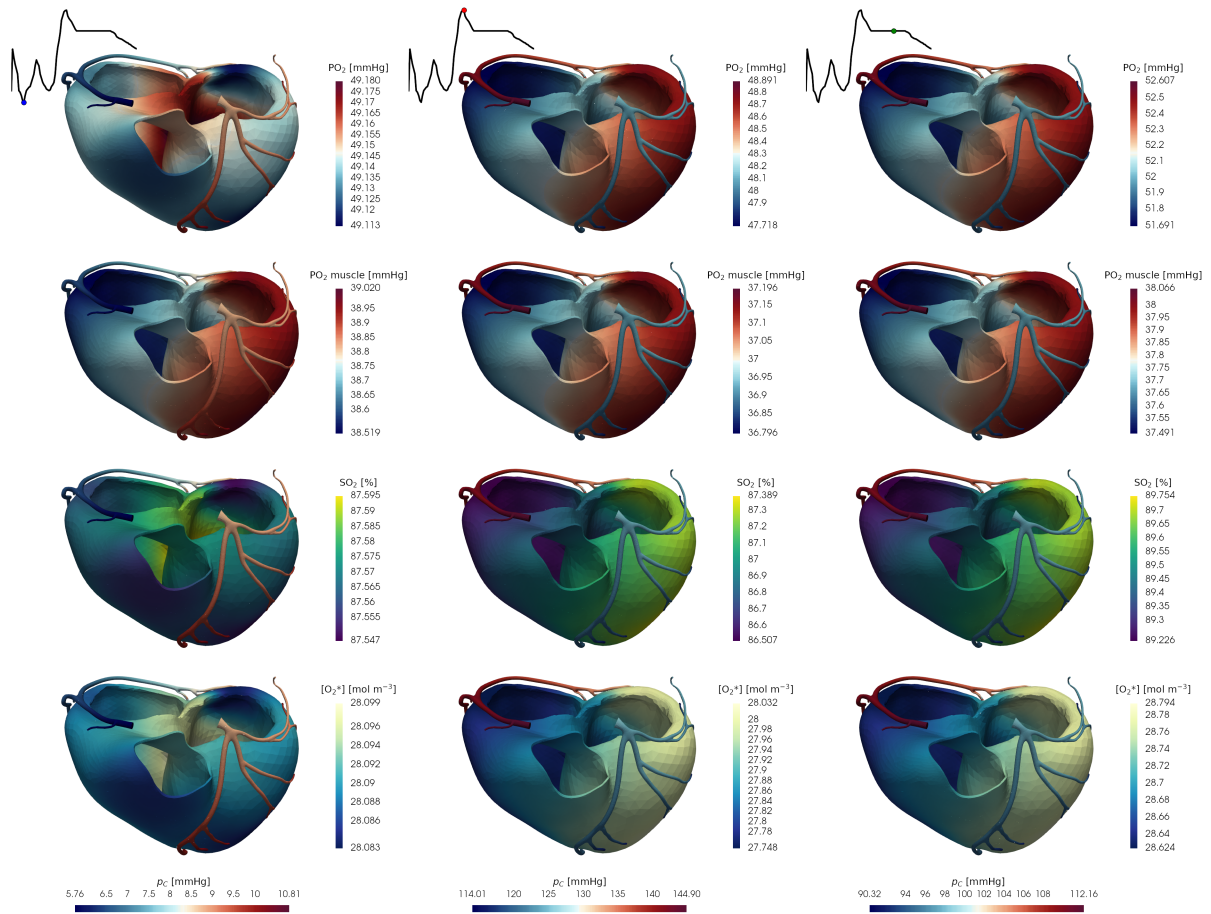


Figure 3: Scalar fields of the multi-physics model in scenario of a healthy subject.

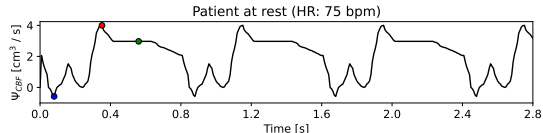


Figure 2: CBF imposed in simulated scenarios.

In Figure 3, we can see the scalar fields p_C in the coronaries and of PO_2^3 , PO_2^m , SO_2^3 and $[\text{O}_2^*]^3$ in the myocardium at the three time steps described above. We notice that, at the beginning systole, the pattern of PO_2^3 differs from the other time steps. The fact that the patterns are similar and that there is no large variability in space confirms that the simulation is following the physiology since we are simulating a healthy system of coronaries and myocardium, adequately supplied by the coronaries in each of its points. For this reason, we can concentrate on the spatially averaged values of the scalar fields, both with the average and total oxygen fluxes, as shown in Figure 4. The model seems in good accordance with the literature [2]: values of SO_2^3 oscillates between 85% and 90%, values of PO_2^m are almost constant near the physiological imposed value of 40 mmHg and the average value of $\lambda_{\text{O}_2}^{\text{cons}}$ of $34 \mu\text{mol L}^{-1} \text{s}^{-1}$, similar to the one available in literature [2, 6].

We also compared the results between real and idealized geometry described above, where inward/outward blood flux was chosen to provide to provide $\Psi_{\text{CBF}} = 0.64 \text{ mL min}^{-1} \text{ g}^{-1}$, near simulated in the coronaries. The results are in good accordance, meaning that not only can the idealized geometry be used instead of the real one, but it is also possible to use the 0D model directly, of course, only in the case of non-pathological tissue. In the case of spacial heterogeneities, such as ischemic regions in the myocardium, this would not be possible without properly simulating the fluid dynamics in coronaries and the blood perfusion in the myocardium.

To study the influence of physical activity, we simulate two cases with the default parameters we used also before, but increasing ξ_0 from 50 mmHg s^{-1} to 130 mmHg s^{-1} to simulate a patient under physical activity. Moreover, we imposed a heartbeat period of 0.65 s for the patient under physical activity. The spatial pattern are similar to the ones in Figure 3, and, looking at the spatially averaged quantities, we notice that an increase in the oxygen consumption by the cardiac muscle affects the model output: in particular, we notice a reduction of SO_2^3 , PO_2^3 , and $[\text{O}_2^*]^3$ caused by hypotension affecting tissue and organs. The value of PO_2^m is near to the imposed one

Var.	m. u.	Physiological value	Pathological value
SO_2^a	%	0.98	0.92
$[\text{Hb}^*]$	mol m^{-3}	10	8.26
PO_2^{50}	mmHg	26.7	23.4
T_{HB}	s	0.8	0.7

Table 1: Pathological parameters to simulate a scenario of SARS-CoV-2 infection.

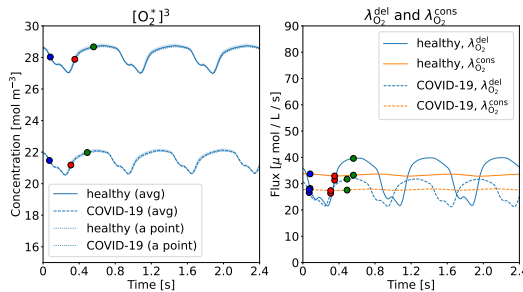


Figure 4: Effects of COVID-19 disease (only $[\text{O}_2^*]^3$ and $\lambda_{\text{O}_2}^{\text{del}}, \lambda_{\text{O}_2}^{\text{cons}}$ depicted).

of 20 mmHg as explained in [6]. The average value of $\lambda_{\text{O}_2}^{\text{cons}}$ rises from $34 \mu\text{mol L}^{-1} \text{s}^{-1}$ of the at rest scenario, to $58 \mu\text{mol L}^{-1} \text{s}^{-1}$, which makes sense since the myocardium needs more oxygen supply from the capillaries to the muscle in order to work properly. Having investigated the scenario of a patient under physical activity, we study the effects of SARS-CoV-2, varying suitable parameters of the model. Hence, we run two simulations with parameters found in the literature for physiological and pathological conditions as in the Table 1. The value of SO_2^a is the minimum saturation level that has to be reached by providing mechanical ventilation to the patient, while the target saturation level for the patient with SARS-CoV-2, provided by the National Institutes of Health (NIH), is of $92\% \div 96\%$ [9]. The value of $[\text{Hb}^*]$ has been selected as the mean value of Hb concentration in SARS-CoV-2 patients computed in the analysis of the Spedali Civili di Brescia, [5] same as the value of the heartbeat period, taken from the same work in which the researchers observed a mean value of cardiac frequency of 85 beat min^{-1} .

Although we simulate a pathological case, we do not affect the coronaries or perfusion problem. Thus, the myocardial tissue is healthy, so we do not expect to obtain spatial heterogeneities. Indeed, notice that, as expected, there are no meaningful pattern differences between the scalar fields and with respect to the scenarios previously presented. We use different time scales again to represent the different time instants so that space variation can be appreciated more. For this reason, we compare the scenarios shown in Figure 4 the spatially averaged quantities, in which we can better analyse the behavior in time, while in Table 2 we can find further details.

Regarding the SO_2^3 , we can see how in the physiological condition, the saturation oscillates between

Var.	m. u.	Healthy			SARS-CoV-2		
		min	avg	max	min	avg	max
PO_2^3	mmHg	44.8	49.6	52.8	34.4	37	39
PO_2^m	mmHg	36.5	37.7	39	26.4	27.1	27.8
SO_2^3	%	84.1	87.8	89.9	77.5	81.3	83.8
$[\text{O}_2^*]^3$	mol m^{-3}	27	28.2	28.9	20.5	21.5	22.2
$\lambda_{\text{O}_2}^{\text{del}}$	$\mu\text{mol L}^{-1} \text{s}^{-1}$	21.6	33.1	39.9	21.2	27.6	32
$\lambda_{\text{O}_2}^{\text{cons}}$	$\mu\text{mol L}^{-1} \text{s}^{-1}$	32.8	33.3	33.8	27.3	27.7	28.1
$\Lambda_{\text{O}_2}^{\text{del}}$	mol L^{-1}	25.1	63.7	105	20.9	54.1	87.1
$\Lambda_{\text{O}_2}^{\text{cons}}$	mol L^{-1}	26.8	66.8	107	22	55.3	88.6

Table 2: Comparison between space-temporal minimum, average and maximum values of healthy and SARS-CoV-2 scenarios.

70%–95%, while in pathological conditions, between 70%–89%, hence in a patient with SARS-CoV-2 the curve is lower than for a healthy one. The plots regarding PO_2^3 show a lower magnitude of the curves in the pathological case for both the quantities considered: this confirms the reduction of partial pressure observed in SARS-CoV-2 patients. On the other hand, the oxygen partial pressure in the muscle is not easily measurable in real cases. Hence, although its reduction makes physical sense in a pathological patient, we do not have a corresponding result in the literature. The oxygen concentration in the pathological case shows a lower curve than in the physiological case but with a similar trend. The value of PO_2^m is, in this case, significantly below the physiological one of 40 mmHg.

Finally, regarding the fluxes of oxygen transported from the capillaries to the tissue and used from muscle to produce ATP, we can notice a reduction in both the quantities for a patient with SARS-CoV-2 infection, a difference which becomes larger and larger the more simulation time we consider. The average value of $\lambda_{\text{O}_2}^{\text{cons}}$ drops from $34 \mu\text{mol L}^{-1} \text{s}^{-1}$ of the at rest scenario, to $28 \mu\text{mol L}^{-1} \text{s}^{-1}$, which makes sense since there is minor oxygen availability.

We conclude by studying the effects of physical activity on a patient affected by SARS-CoV-2 infection. In order to do so, we used the pathological parameters listed in Table 1 both with $\xi_0 = 130 \text{ mmHg s}^{-1}$. Again, for the previously described reasons, there are no meaningful pattern differences in the model output. Regarding the spatially averaged quantities, we notice that also, in this case, we have more delivered oxygen, as explained before. The average value of $\lambda_{\text{O}_2}^{\text{cons}}$ rises from $28 \mu\text{mol L}^{-1} \text{s}^{-1}$ of the at rest scenario, to $49 \mu\text{mol L}^{-1} \text{s}^{-1}$, but remaining lower than the value of the healthy subject under physical activity, which was $58 \mu\text{mol L}^{-1} \text{s}^{-1}$, due to SARS-CoV-2 infection. Although apparently in good condition, a patient with SARS-CoV-2 infection has a smaller oxygen reserve: thus, starting to perform physical activity can be particularly dangerous since it can suddenly provide an oxygen deficit.

5. Conclusions and further developments

In this work, an innovative oxygenation model was derived, describing the biological parameters involved. The model was coupled with the other physics of blood dynamics in epicardial coronary arteries and intramural coronary vessels, discretized in 0D and 3D cases, and then implemented inside the high-performance computing library `lifex`. We performed some numerical which validated the solver and, in this context, we also tuned some physical parameters to improve the model's accordance with the literature and make the model solutions quickly reach a limit cycle. Finally, we used the coupled model to simulate real-life scenarios of realistic coronaries and myocardium geometries. The model allows for simulating blood dynamics in epicardial coronary arteries that perfuses the myocardium porous medium, which idealizes the intramural coronary vessels, and finally to obtain the spatial-temporal evolution of the oxygenation values in the myocardium capillaries. This pipeline provided very detailed information about the oxygenation level in the patient. It allowed us to study the differences between a healthy subject and a patient with Sars-CoV-2 infection and assess the effect of physical activity on both of these patients. The results of these comparisons appeared to be in great accordance with the literature confirming the model's soundness and showed to which parameters the model is most sensitive.

This work can lead to many future developments and further research. Instead of the Michaelis-Menten model for muscle dynamics, we can couple the oxygenation model with a model of cellular metabolism. The latter one, in turn, can be coupled with another model describing how the stored energy can be transformed in work to make the muscle contract. We could also use the results of the oxygenation model to improve the physical accuracy of other models: as an instance, instead of assuming an optimal value of oxygen concentration in the blood, a fluid dynamics problem could use the real one provided by the oxygenation model. This way, the fluid viscosity is better estimated, so the simulation reaches better accuracy. Although we simulated a pathological scenario, the disease only impacted the oxygenation model. Hence the myocardial tissue remained healthy, so there were no spatial heterogeneities. It would be interesting to study the differences in oxygenation curves when the myocardium presents some ischemic regions or in the case of some coronaries syndromes. Finally, another possible goal would be to use this multi-physics model on patient-specific geometries of coronaries and myocardium, to provide each patient with a digital-twin that helps diagnose and predict complex pathologies.

References

- [1] P. C. Africa. `lifex`: a flexible, high performance library for the numerical solution of complex finite element problems, 2022. URL <https://lifex.gitlab.io/>.
- [2] Deranged Physiology. Myocardial oxygen supply and demand, 2020. URL <https://bit.ly/3AqzuXJ>. [Online, accessed in September 2022].
- [3] S. Di Gregorio, M. Fedele, G. Pontone, A. F. Corno, P. Zunino, C. Vergara, and A. Quarteroni. A multiscale computational model of myocardial perfusion in the human heart. *MOX Report 2019/48, Politecnico di Milano*, 2019.
- [4] D. Goldman. Theoretical models of microvascular oxygen transport to tissue. *Microcirculation*, 15(8):795–811, 2008. doi: 10.1080/10739680801938289. PMID: 18608981.
- [5] R. M. Inciardi et al. Characteristics and outcomes of patients hospitalized for Covid-19 and cardiac disease in northern italy. *European Heart Journal*, 41(19):1821–1829, 2020.
- [6] G. Jenkins, C. Kemnitz, and G. J. Tortora. *Anatomy and Physiology: From Science to Life—Second (2nd) Edition*. Wiley, 2009.
- [7] A. Quarteroni, L. Dede', A. Manzoni, and C. Vergara. *Mathematical Modelling of the Human Cardiovascular System: Data, Numerical Approximation, Clinical Applications*. Cambridge Monographs on Applied and Computational Mathematics. Cambridge University Press, 2019. doi: 10.1017/9781108616096.
- [8] F. Regazzoni. Oxygen exchange model. *Internal MOX Report, Politecnico di Milano*, 2020.
- [9] N. Shenoy, R. Luchtel, and P. Gulani. Considerations for target oxygen saturation in Covid-19 patients: are we under-shooting? *BMC Medicine*, 18(1):1–6, 2020.